Graphene Earphones: Entertainment for Both Humans and Animals

He Tian, Cheng Li, Mohammad Ali Mohammad, Ya-Long Cui, Wen-Tian Mi, Yi Yang, Dan Xie, and Tian-Ling Ren*

Institute of Microelectronics and Tsinghua National Laboratory for Information Science and Technology (TNList), Tsinghua University, Beijing 100084, China

ABSTRACT

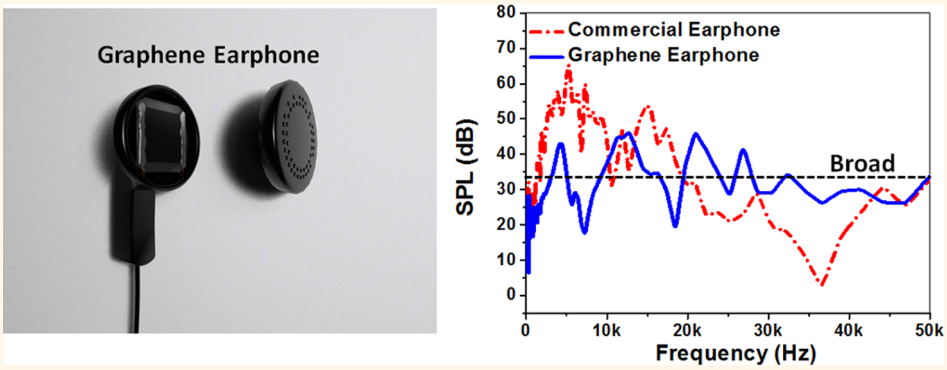

The human hearing range is from 20 Hz to 20 kHz. However, many animals can hear much higher sound frequencies. Dolphins, especially, have a hearing range up to 300 kHz. To our knowledge, there is no data of a reported wide-band sound frequency earphone to satisfy both humans and animals. Here, we show that graphene earphones, packaged into commercial earphone casings can play sounds ranging from 100 Hz to 50 kHz. By using a one-step laser scribing technology, wafer-scale flexible graphene earphones can be obtained in 25 min. Compared with a normal commercial earphone, the graphene earphone has a wider frequency response (100 Hz to 50 kHz) and a three times lower fluctuation (±10 dB). A nonlinear effect exists in the graphene-generated sound frequency spectrum. This effect could be explained by the DC bias added to the input sine waves which may induce higher harmonics. Our numerical calculations show that the sound frequency emitted by graphene could reach up to 1 MHz. In addition, we have demonstrated that a dog wearing a graphene earphone could also be trained and controlled by 35 kHz sound waves. Our results show that graphene could be widely used to produce earphones for both humans and animals.

KEYWORDS: graphene · earphone · acoustic device · laser scribing · graphene oxide · human–animal communication · frequency response

Communication between humans and animals is of great importance.[1−3] For this purpose, studying the languages of various intelligent species, such as dolphins, has attracted a lot of attention.[4−6] However, there is a sound frequency band mismatch between humans and various animals of interest. Humans can hear sound frequencies ranging from 20 Hz to 20 kHz.[7] However, animals can communicate in a larger frequency range over 20 kHz in the ultrasonic range. Bats, for instance, produce high-pitched sounds measured from as low as 10 kHz to higher than 160 kHz. People with acute hearing can hear a part of the lower range of bat sounds, but most bat sounds are beyond the human range. Philippine tarsiers, among the world's tiniest primates, use ultrasound for communication. Their calls have been documented at 90 kHz when reaching their highest frequency. Some whales can emit signals as high as 175 kHz. Dolphins, in particular, generate sounds that could reach up to 300 kHz. However, current earphones designed merely for human entertainment range from 20 Hz to 20 kHz.[8] Ultrasound transducers,[9−11] which operate at frequencies higher than 20 kHz, are produced based on the piezoelectric effect. The aforementioned devices produce sound based on membrane vibrations, and therefore, the sound frequency response has its resonance peaks. As a result, there is no

* Address correspondence to RenTL@tsinghua.edu.cn.

Received for review February 16, 2014 and accepted April 26, 2014.

Published online April 26, 2014
10.1021/nn5009353

data reported on wide-band sound frequency earphones simultaneously covering the hearing range of both humans and animals. In order to bridge this gap between humans and animals, it is necessary to find a universal earphone based on new materials.

Recently, electro-thermoacoustic (ETA) devices have attracted a lot of attention.[12,13] ETA devices use an ultrathin conductive layer (Al, CNT, *etc.*) to emit sound. However, in contrast to the mechanism employed in conventional audio frequency earphones or ultrasonic transducers, there is no displacement of the surface in ETA devices. In response to an alternating current (AC) signal, the ETA device surface heats up and warms the air molecules near the surface. These air molecules transfer their energy to adjacent molecules and so on. This cascading process generates sound waves. ETA devices introduce new opportunities to realize earphones with a wide-band frequency response. In order to make high-performance ETA devices, three conditions should be met. First, the conductor should be thin enough with a low thermal capacity per unit area. Second, the conductor should be suspended to prevent thermal leakage from the substrate. Third, the conductor area should be large enough (*e.g.*, 1 cm^2) to build a sufficient sound field. Graphene has been previously used to demonstrate sound emission.[14−18] Almost all of the graphene films used for previous sound emission experiments were grown by chemical vapor deposition (CVD), which requires many hours for film growth, transfer, and subsequent patterning of the transferred film. Furthermore, graphene grown by CVD has a planar structure and is attached to the substrate due to van der Waals forces. The thermal conductivity of the substrate is much higher than that of air. As a result of this contact, more than 90% of heat is lost from the substrate.[12] In order to prevent thermal leakage, porous substrates (filter paper,[14] anodic aluminum oxide,[15] porous silicon oxide[16]) have been used. However, this approach requires a complex fabrication process and yields a suspended graphene structure resulting in a low yield.

Here, a time-efficient approach to fabricate graphene earphones using laser-scribed graphene (LSG) is experimentally demonstrated. The laser-scribed region resembles a foam-like structure containing polycrystalline graphene. The main advantage of the LSG is that air gaps exist between the graphene layers which benefits thermoacoustic sound emission by preventing thermal leakage from the substrate. The graphene earphone is packaged as a commercial earphone and can play music. In this work, a graphene earphone with a sound frequency ranging from 100 Hz to 50 kHz is shown, which could be useful for both humans and animals. As compared to a commercial earphone, the graphene earphone has a relatively flat frequency response due to its resonance-free oscillation. A theoretical model based on the ETA effect fits well with our experimental results. Moreover, a dog wearing the graphene earphone could also be trained and controlled by 35 kHz sound waves, as demonstrated in this work. The results show that graphene could be widely used as an earphone for various species.

RESULTS

A mask-free and programmable laser scribing technology is employed to obtain ultrafast graphene growth at precise locations. A schematic diagram of the graphene earphone fabrication process is shown in Figure 1a (see the Methods section for details). A graphene oxide (GO) film is applied on a polyethylene terephthalate (PET) film-coated DVD media disk. The disk is inserted into a LightScribe DVD drive to pattern a given design by laser-induced reduction of the GO into graphene films.[19] The 788 nm laser inside the drive reduces the golden-brown GO into black graphene at precise locations. This laser scribing technology makes it possible for wafer-scale precise graphene patterning in ~25 min. For example, original images of the Tsinghua University gate are imported into the DVD drive. Several minutes later, the same images are reproduced on the LSG (Supporting Information Figure S1). With laser scribing, wafer-scale flexible graphene earphones on the PET substrate could be realized (Figure 1b). The inset of Figure 1b shows the graphene earphones at 1 cm^2 dimensions.

The morphology and structure of graphene sheets are also shown (Figure 1c). Before the laser scribing, the GO film is quite flat and dense. After the laser scribing, a graphene film of 10 μm thickness is obtained (Figure S2). It is noticed that there is an almost 10-fold thickness increase for the LSG compared to the original GO film. Such a phenomenon is quite different from the conventional reduction results of GO, which could lead to the decrease in the final film thickness. In the case of the LSG, the thickness increase is due to the short-time laser pulses on a small area of GO, which may generate oxygen rapidly and result in expanding the layer to layer spacing. Such a process has a similar effect to thermal shocking. The electrical resistance before and after the laser scribing are 580 MΩ and 8.2 kΩ, respectively. There is an almost 5 orders of magnitude reduction in resistance as a result of the laser scribing. The film characteristics after laser scribing are presented in the Supporting Information Figures S3−S6, which includes results after Raman spectroscopy, XPS, optical microscopy, and electrical testing (sheet resistance).

The LSG earphone is packaged successfully into a commercial earphone casing by replacing a conventional voice coil speaker. After the laser scribing of the wafer-scale graphene patterns, these patterns could be cut into individual graphene earphones. Figure 2a presents an individual graphene earphone with an area of 10 × 10 mm^2. Silver paste is applied on both sides of the graphene film to establish electrical input.

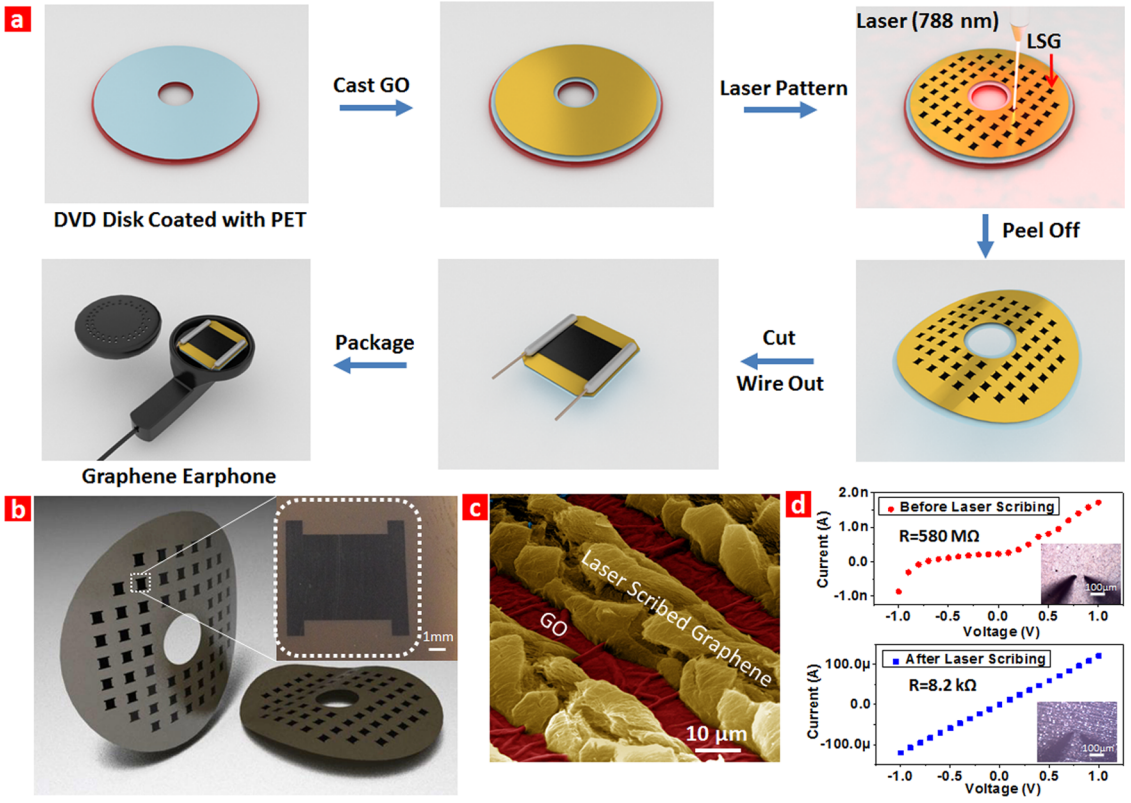

Figure 1. Laser scribing technology for flexible graphene earphone fabrication. (a) Process flow of the graphene earphone fabrication. (b) Wafer-scale flexible graphene earphones. The inset shows an optical microscope image of the LSG earphone. (c) SEM image of the LSG and GO in false color. (d) Electrical properties before and after laser scribing.

Figure 2. Graphene earphone. (a) Graphene earphone in hand. (b) View of the graphene earphone in a commercial earphone casing. (c) Exploded view of a packaged graphene earphone. (d) A pair of graphene earphones in its final packaged form.

The graphene earphones are finally connected to the electrical wiring of a commercial earphone casing using copper wires (Figure 2b). The structure of the graphene earphone is shown with the top cap, graphene sheets, Ag electrodes, PET, and the bottom cap (Figure 2c). One of the most striking features is that the graphene earphone is significantly thinner than a voice coil. A pair of packaged graphene earphones for human use (Figure 2d) is indistinguishable from a generic set of earphones; however, due to the membrane-like structure of the graphene earphones, even thinner earphones can be designed in the future. In order to get a satisfying sound intensity, a drive circuit is designed to amplify the input electrical signal (Figure S7). It is worth mentioning that the input sound frequency is doubled due to the ETA effect, and this needs to be compensated during actual testing, as described ahead. The drive circuit uses a USB port to apply power to the circuit for amplifying the AC signal and also to apply an up to 15 V DC bias to the graphene earphone (Figure S8). In this way, the graphene earphone can connect to a laptop for playing music.

The graphene earphone developed in this work has the potential to bring a revolution in the field of acoustics. In order to compare our graphene earphone with a commercial earphone, both are tested by the same audio analysis system. The audio analyzer sweeps the sound frequency from 100 Hz up to 50 kHz, carrying sine signals to drive the earphone and the standard microphone, and captures the acoustic response accordingly. Figure 3a presents the experimental setup. The graphene earphone is placed 1 cm away from the standard microphone. The standard microphone converts the sound generated from graphene into electrical signals. As shown in Figure 3b, the graphene earphone exhibits a reasonably flat frequency response in a wider frequency range (100 Hz to 50 kHz).

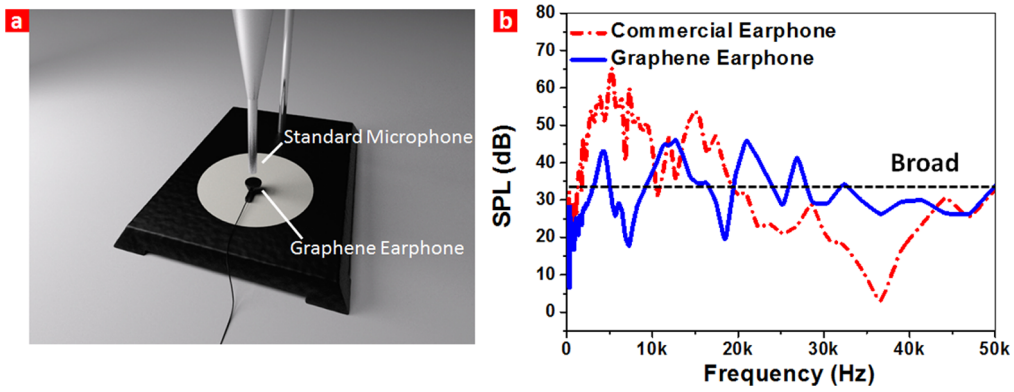

Figure 3. Sound pressure and frequency characteristics of the graphene earphone. (a) Experimental setup for the graphene earphone. (b) Sound pressure level (SPL) curves of a graphene earphone compared with a commercial earphone. It is observed that the graphene earphone has a lower fluctuation than a commercial earphone due to its resonance-free oscillation.

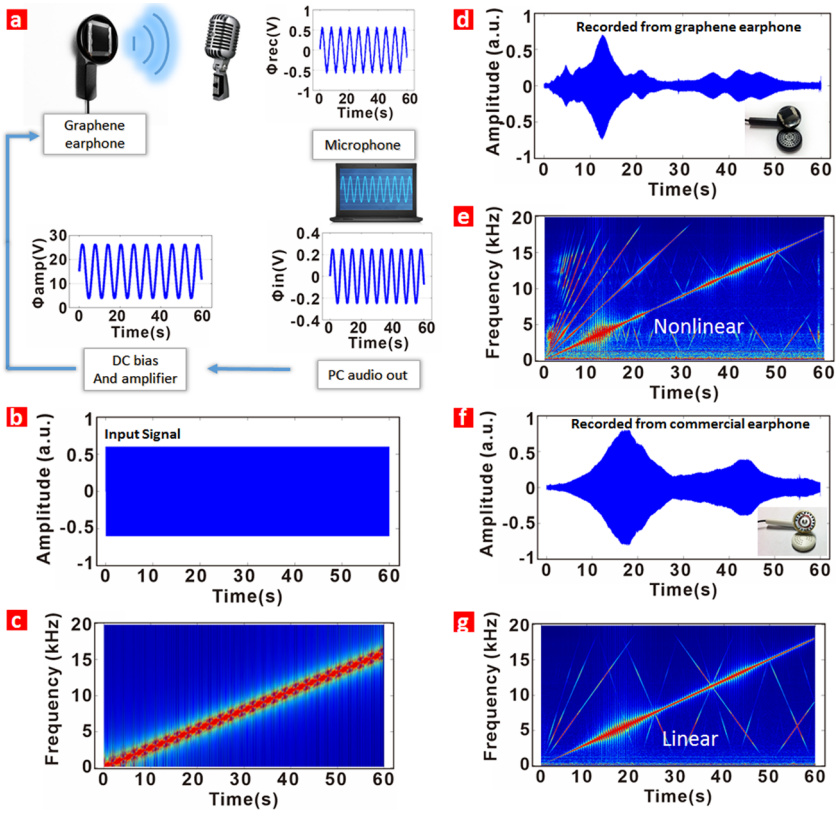

Figure 4. Graphene earphone testing results in the time and frequency domains. (a) Experimental setup for testing the graphene earphone in the audio frequency range. The amplitude spectrum (b) and its Fourier transform (c) for a constant amplitude sine wave sweep from 0 to 20 kHz. The colors represent the intensity of the frequency, with warmer colors indicating a higher intensity. The amplitude spectrum (d) and its Fourier transform (e) of the sound generated by the graphene earphone. The inset in panel (d) shows the graphene earphone. There is an obvious nonlinear effect in the graphene earphone. The amplitude spectrum (f) and its Fourier transform (g) of the sound generated by a commercial earphone. The inset in panel (f) shows the commercial earphone based on magnetic coils. The sound frequency is linear.

Note that the 50 kHz limitation is due to our measurement system. The graphene earphone can produce even higher sound frequencies. However, the commercial earphone presents strong resonance peaks at 5.3 kHz followed by a severe attenuation in the sound intensity beyond 20 kHz. Meanwhile, the sound intensity of the graphene earphone remains relatively stable. Compared with a normal commercial earphone with a fluctuation of ±30 dB, the graphene earphone presents a much lower fluctuation of ±10 dB. We believe this is caused by the resonance-free oscillations of the graphene earphone. Such a phenomenon shows that the graphene earphone could be widely used in various acoustic applications. Since the casing of the graphene earphone can affect the sound distribution, the graphene sound performance before packaging is

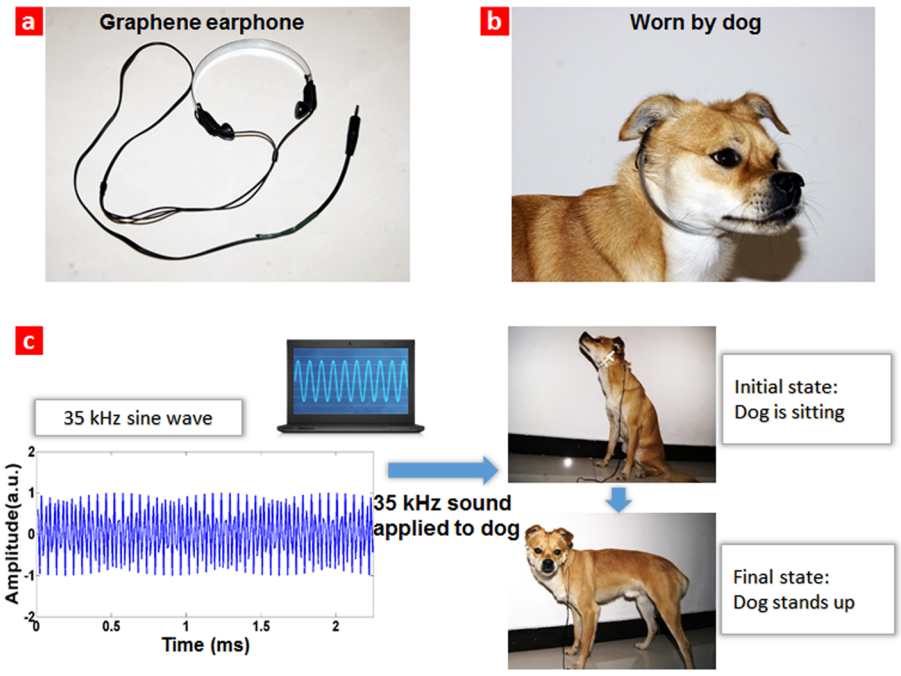

Figure 5. Animal subject responding to ultrasound signal through graphene earphones. (a) Graphene earphones suitable for a dog subject. (b) Subject wearing the graphene earphone. (c) Communication with the subject through the earphone in ultrasound. The dog is initially sitting down. After receiving a familiar 35 kHz signal, it stands up.

also tested to know its original sound properties. After the graphene film is packaged into the standard earphone casing containing small holes, there is a Helmholtz resonance in the casing cavity (see Supporting Information Figure S9). This also indicates that carefully designing the casing or the top cap of the casing could yield a more stable frequency response.

In the audio range, the time domain response of the graphene earphone is also investigated and compared to a regular earphone. The experimental setup is presented in Figure 4a. A personal computer is used to produce linear sine sweep signals (see Figure S10 to inspect detailed features). After an amplification of 30 times, the signals are fed to the graphene earphone. The sound signals are subsequently recorded by a microphone. The time and frequency domain representations of the input signals (linear sine sweep from 0 to 20 kHz) are shown in Figure 4b,c. The recorded output from the graphene earphone is presented in Figure 4d. After the signals are transferred into the frequency domain, higher-order harmonics are observed (Figure 4e). Such a nonlinear effect may be due to the DC bias that is applied to the input sine waves. As described previously, a drawback of the ETA effect is that the output sound frequency is twice as large as the input signal. In order to recover the same frequency as the input signal, a DC bias is added. In the frequency domain, the effect of this DC bias is to generate the fundamental tone and many higher-order harmonics which distort the output (Figure 4e). In order to generate a single-frequency tone without distortion caused by higher-order harmonics, the graphene earphone could be driven using pulse density modulation.[20]

In comparison, a linear frequency response is observed from a commercial earphone (Figure 4f,g) due to the resonance oscillation mechanism. Conventional earphones are based on mechanical damping of a thin membrane. When alternating current passes through the magnetic coil, the connected membrane can oscillate. The air near the membrane surface is compressed or expanded adiabatically. Therefore, a solely volumetric change of air is occurring without the generation of any heat. In such a mass-spring system, the output sound frequency has a linear relation with the input signal. However, the amplitude response is frequency-dependent due to the resonance of the film. For this reason, a wide-band frequency response cannot be realized by a conventional earphone.

Finally, an application of the graphene earphone is demonstrated. It is universally known that dogs can be trained to understand human commands and take the desired action. However, electronic communication at ultrasonic frequencies may be required under various circumstances (high noise or battlefield environments, *etc.*). We would like to demonstrate a proof-of-concept electronic intraspecies communication at ultrasonic frequencies using the graphene earphone. The hearing range of dogs is usually around 30 Hz to 60 kHz. The graphene earphone is attached to a steel structure (Figure 5a) so that a dog can wear it (Figure 5b). A previously trained dog is subjected to a new conditioning such that the dog stands up after hearing a 35 kHz sine wave (see details in Supporting Information S11).

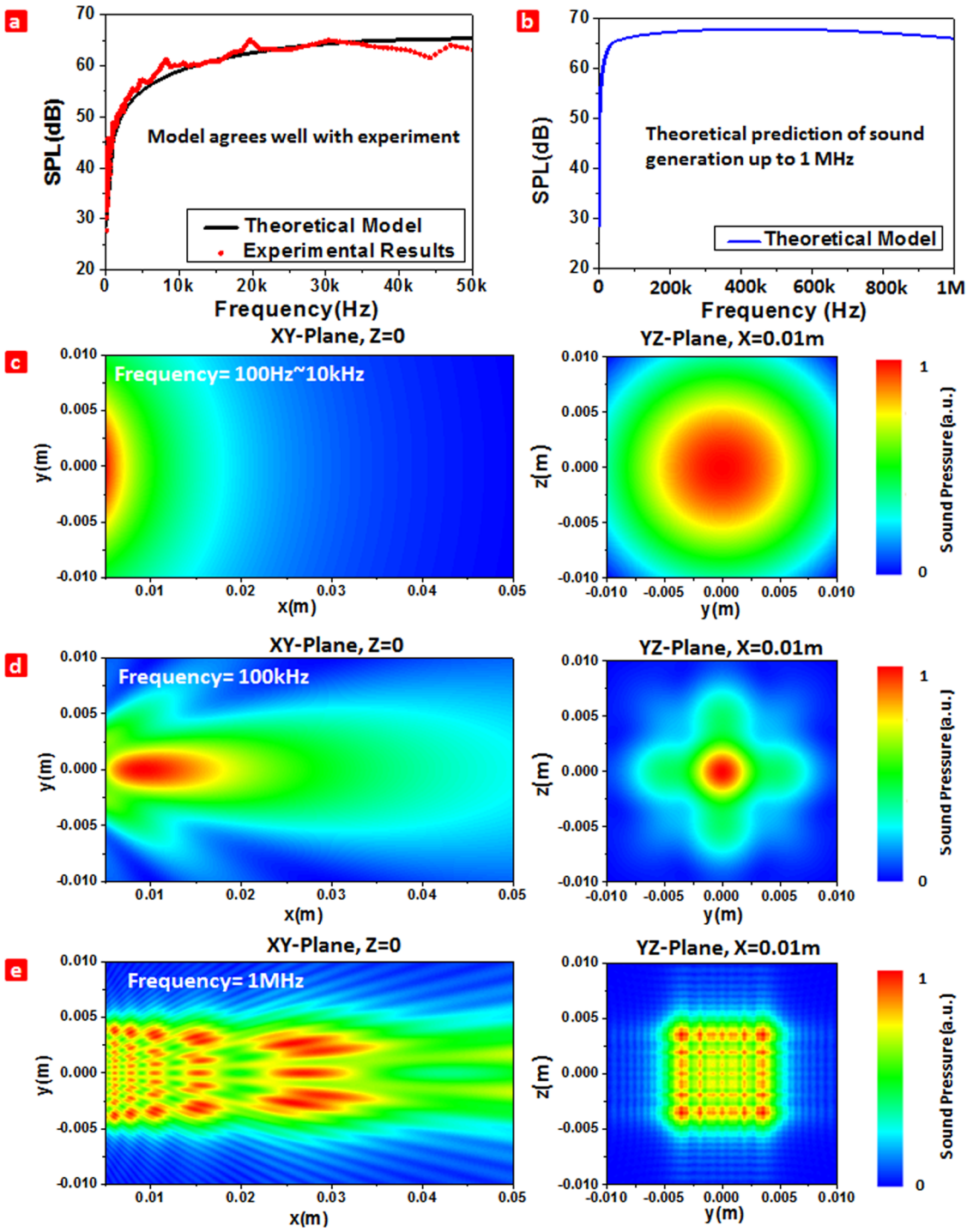

Figure 6. Simulation of the graphene earphone with a performance range from 100 Hz to 1 MHz. (a) SPL *vs* frequency showing that the model agrees well with experiment up to a frequency of 50 kHz. (b) SPL *vs* frequency showing the graphene can realize sound generation of up to 1 MHz. The sound pressure distributions in the *XY* and *YZ* planes calculated using eq 1 at (c) 100 Hz−10 kHz; (d) 100 kHz; and (e) 1 MHz.

The sample rate used in this experiment is 88 200 samples per second (more than 2 × 35 kHz), which ensures that the acoustic signal is transmitted well.[21] At first, the dog was ordered to sit down (Figure 5c). After a short pause, a 35 kHz sine wave was played to the dog, and it stands up as expected (see Supporting Information video S1). The dog was unharmed during testing.

DISCUSSION

The graphene earphone is analyzed based on the ETA effect (Figure S12). For a point sound source, the output sound can be written as[22]

$$\Delta p_{air}(\bar{r}, f_{th}) = \frac{3 \times P_{eleff} \times f_{th}}{4 \times \pi \times c_{air}^2 \times |\bar{r}|} \times E_{air} \times A_{air} \quad (1)$$

where P_{eleff} is the effective value of the supplied electric power, f_{th} is the thermal excitation frequency, c_{air} is the specific heat capacity of air, $\bar{r}$ is the measured distance from the sound source, E_{air} is the energy distribution coefficient of air, and A_{air} is the sound attenuation factor.

For a square sound source, the graphene surface has to be discretized into n point sources. Using point source synthesis, a discretized version of the Kirchhoff–Helmholtz integral can be written where the complex amplitude of all n point sources will be superimposed at the sound measurement point r.[22]

$$\Delta p_{air}(\bar{r}, f_{th}) = \sum_{k=1}^{k=n} \Delta p_{air,k}(\bar{r}_k, f_{th}) \times \left| \exp\left(i \times 2 \times \pi \times \frac{|\bar{r}_k| \times f_{th}}{c_{air}} \right) \right| \quad (2)$$

In eq 2, $\Delta p_{air,k}(\bar{r}_k, f_{th})$ is the sound intensity from the point k, and all other variables and constants have the same meanings as in eq 1.

By solving eq 2, the behavior of the graphene earphone can be predicted as shown in Figure 6. The sound pressure level (SPL) *versus* the frequency plot shows that the model agrees well with experiment up to 50 kHz. This result shows that the working principle of the graphene earphone is indeed based on the ETA effect (see Supporting Information Figure S13). Consequently, the high-frequency range can also be evaluated using this theory. The theoretical SPL plot shows that sounds up to 1 MHz may be generated using the graphene earphone. Moreover, the sound pressure distributions of the graphene earphone could also be found in Figure 6c–e. From 100 Hz to 10 kHz, the sound is emitted in a 180° spread with low directivity, which could be regarded as a point sound source. After the frequency is increased to 100 kHz, the directivity is enhanced. Eventually at 1 MHz, the sound field diffraction is observed due to the short sound wavelength.

The graphene earphone has several advantages compared to the AI[12,23,24] and CNT[13,25–30] ETA devices. Since air gaps exist between the LSG layers, thermal leakage from the substrate is minimized from the substrate (Figure S14). Moreover, the LSG is fabricated relatively easily using a one-step laser scribing technology. This mask-free and programmable patterning method ensures that graphene is directly grown on a PET substrate without transfer and photoresist contamination. Finally, the graphene earphone is found to be a suitable communication device to bridge the gap between humans and animals due to its exceptional frequency range.

CONCLUSION

In this work, wafer-scale graphene earphones have been realized using laser scribing technology. Sound generation from the LSG has been demonstrated in frequencies ranging from 100 Hz to 50 kHz. In comparison to a commercial earphone, the graphene earphone has a relatively flat frequency response and a lower sound pressure fluctuation. However, the ETA effect gives rise to nonlinear (harmonic) distortion most likely caused due to the addition of a DC bias in the input signal for the purpose of recovering the input (fundamental) frequency. Theoretical calculations predict that the graphene earphone may operate at frequencies as high as 1 MHz. Finally, a dog was trained to respond to an ultrasound (35 kHz) signal fed to it using a graphene earphone. This work shows that earphones developed using graphene could make full use of the hearing range in both humans and various animals of interest, therefore opening up a whole new way of interspecies communication.

METHODS

Material Preparation. A common Hummers method was used to synthesize a GO dispersion with a 2 mg/mL concentration using graphite powder provided by XFNANO Materials Tech Co., Ltd. (Nanjing, China). An approximately 10 mL GO solution was cast on the surface of the laser-scribed DVD disk coated with PET. The GO solution was left overnight to dry on the DVD disk resulting in an approximately 1 μm thickness.

Fabrication Process of Graphene Earphone. The fabrication of graphene earphones (Figure 1a) relies on laser reduction of the GO film.[31–34] The GO/PET-coated DVD disk was patterned by a LightScribe DVD drive (HP Inc. 557S). The laser of this DVD drive has a power of 5 mW, a wavelength of 788 nm, a spot size of 6 μm, and a dwell time of 0.1 s. Graphene earphone patterns were designed by L-Edit layout software and transferred to the coated DVD disk using the Nero StartSmart software. In this way, wafer-scale patterning of graphene earphones can be performed in ~25 min. After the laser fabrication, the PET substrate can be peeled off the disk and the graphene earphones can be cut out. These earphones are wired out by copper wire using silver paste and finally packaged in a conventional earphone casing.

Characterization. The surface morphology of the LSG is observed by a Quanta FEG 450 SEM (FEI Inc.) and a JEM-2010 TEM (JEOL Inc.). Raman spectroscopy is performed using a laser with a wavelength of 532 nm (HORIBA Inc.).

Testing of the Graphene Earphone. The acoustic platform for testing the LSG earphones consisted of a standard microphone and a dynamic signal analyzer. A 1/4 in. standard microphone (Earthworks M50) was used to measure the sound pressure level of the loudspeakers. This microphone has a very flat frequency response reaching up to 50 kHz and a 31 mV/Pa high sensitivity. A signal analyzer (Agilent 35670A) was used to generate sine signals to drive the earphones, perform fast Fourier transform analysis, and record the value of the sound pressure level. Our testing was performed in a soundproof box measuring $1.0 \times 0.5 \times 0.5$ m^3. In order to avoid echo, the box was filled with sound-absorbing sponges.

Simulation of the Graphene Earphone. For the theoretical calculation of sound pressure amplitudes at a fixed distance, Figure 6a,b is plotted using eq 2 while varying the thermal excitation frequency f_{th}. For mapping of sound pressure amplitudes at a fixed frequency, Figure 6c–e is plotted using eq 2 while varying the distance r.

Conflict of Interest: The authors declare no competing financial interest.

Acknowledgment. This work was supported by the National Natural Science Foundation of China (61025021, 60936002, 51072089, and 61020106006), the National Key Project of Science and Technology (2011ZX02403-002), and the Special Fund for Agro-scientific Research in the Public Interest (201303107). H.T. is additionally supported by the Ministry of Education Scholarship of China, and M.A.M. is supported by the postdoctoral fellowship (PDF) program of the Natural Sciences and Engineering Research Council of Canada (NSERC).

Supporting Information Available: Testing results and discussion of graphene earphones. This material is available free of charge *via* the Internet at http://pubs.acs.org.

REFERENCES AND NOTES

1. Haldane, J. B. S. Animal Communication and the Origin of Human Language. *Sci. Prog.* **1955**, *43*, 385–401.
2. Ojemann, G. A.; Creutzfeldt, O. D. Language in Humans and Animals: Contribution of Brain Stimulation and Recording. *Compr. Physiol.* **1987**, 675–699.
3. Noske, B. *Beyond Boundaries: Humans and Animals*; Black Rose Books Ltd.: Montreal, Canada, 1997; pp 58−78.
4. Van Schaik, C. Why Are Some Animals So Smart? *Sci. Am.* **2006**, *294*, 64–71.
5. Morell, V. Minds of Their Own: Animals Are Smarter Than You Think. *Natl. Geogr.* **2008**, *231*, 36–61.
6. Gregg, J. *Are Dolphins Really Smart? The Mammal Behind the Myth*. Oxford University Press: Oxford, UK, 2013; pp 11−20.
7. Wold, E.; Blum, T.; Keislar, D.; Wheaten, J. Content-Based Classification, Search, and Retrieval of Audio. *IEEE MultiMedia* **1996**, *3*, 27–36.
8. Nakazawa, M.; Nishikata, A. Development of Sound Localization System with Tube Earphone Using Human Head Model with Ear Canal. *IEICE Trans. Fundam. Electron. Commun. Comput. Sci.* **2005**, *88*, 3584–3592.
9. Muralt, P.; Ledermann, N.; Paborowski, J.; Barzegar, A.; Gentil, S.; Belgacem, B.; Petitgrand, S.; Bosseboeuf, A.; Setter, N. Piezoelectric Micromachined Ultrasonic Transducers Based on PZT Thin Films. *IEEE Trans. Ultrason. Ferroelectr. Freq. Control* **2005**, *52*, 2276–2288.
10. Zhu, Y.-P.; Ren, T.-L.; Yang, Y.; Wu, X.-M.; Zhang, N.-X.; Liu, L.-T.; Tan, Z.-M.; Wang, H.-N.; Cai, J.; Wang, S.-D. Novel Ferroelectrics-Based Micro-acoustic Devices and Their Ultrasonic Applications. *IEEE Int. Electron Devices Meet.* **2004**, 51–54.
11. Ren, T.-L.; Zhu, Y.-P.; Yang, Y.; Wu, X.-M.; Zhang, N.-X.; Liu, L.-T.; Li, Z.-J. Micro Acoustic Devices Using Piezoelectric Films. *Integr. Ferroelectr.* **2006**, *80*, 331–340.
12. Shinoda, H.; Nakajima, T.; Ueno, K.; Koshida, N. Thermally Induced Ultrasonic Emission from Porous Silicon. *Nature* **1999**, *400*, 853–855.
13. Xiao, L.; Chen, Z.; Feng, C.; Liu, L.; Bai, Z.-Q.; Wang, Y.; Qian, L.; Zhang, Y.; Li, Q.; Jiang, K. Flexible, Stretchable, Transparent Carbon Nanotube Thin Film Loudspeakers. *Nano Lett.* **2008**, *8*, 4539–4545.
14. Tian, H.; Ren, T.-L.; Xie, D.; Wang, Y.-F.; Zhou, C.-J.; Feng, T.-T.; Fu, D.; Yang, Y.; Peng, P.-G.; Wang, L.-G. Graphene-on-Paper Sound Source Devices. *ACS Nano* **2011**, *5*, 4878–4885.
15. Tian, H.; Xie, D.; Yang, Y.; Ren, T.-L.; Wang, Y.-F.; Zhou, C.-J.; Peng, P.-G.; Wang, L.-G.; Liu, L.-T. Single-Layer Graphene Sound-Emitting Devices: Experiments and Modeling. *Nanoscale* **2012**, *4*, 2272–2277.
16. Suk, J. W.; Kirk, K.; Hao, Y.; Hall, N. A.; Ruoff, R. S. Thermoacoustic Sound Generation from Monolayer Graphene for Transparent and Flexible Sound Sources. *Adv. Mater.* **2012**, *24*, 6342–6347.
17. Tian, H.; Xie, D.; Yang, Y.; Ren, T.-L.; Wang, Y.-F.; Zhou, C.-J.; Peng, P.-G.; Wang, L.-G.; Liu, L.-T. Static Behavior of a Graphene-Based Sound-Emitting Device. *Nanoscale* **2012**, *4*, 3345–3349.
18. Tian, H.; Yang, Y.; Xie, D.; Ge, J.; Ren, T.-L. A Reduced Graphene Oxide Sound-Emitting Device: A New Use for Joule Heating. *RSC Adv.* **2013**, *3*, 17672–17676.
19. Tian, H.; Yang, Y.; Xie, D.; Cui, Y. L.; Mi, W. T.; Zhang, Y. G.; Ren, T. L. Wafer-Scale Integration of Graphene-Based Electronic, Optoelectronic and Electroacoustic Devices. *Sci. Rep.* **2014**, *4*, 3598.
20. Koshida, N.; Hippo, D.; Mori, M.; Yanazawa, H.; Shinoda, H.; Shimada, T. Characteristics of Thermally Induced Acoustic Emission from Nanoporous Silicon Device under Full Digital Operation. *Appl. Phys. Lett.* **2013**, *102*, 4.
21. Shannon, C. E. Communication in The Presence of Noise. *Proc. IRE* **1949**, *37*, 10–21.
22. Daschewski, M.; Boehm, R.; Prager, J.; Kreutzbruck, M.; Harrer, A. Physics of Thermo-acoustic Sound Generation. *J. Appl. Phys.* **2013**, *114*, 114903.
23. Niskanen, A.; Hassel, J.; Tikander, M.; Maijala, P.; Gronberg, L.; Helisto, P. Suspended Metal Wire Array as a Thermoacoustic Sound Source. *Appl. Phys. Lett.* **2009**, *95*, 163102.
24. Vesterinen, V.; Niskanen, A.; Hassel, J.; Helisto, P. Fundamental Efficiency of Nanothermophones: Modeling and Experiments. *Nano Lett.* **2010**, *10*, 5020–5024.
25. Kozlov, M. E.; Haines, C. S.; Oh, J.; Lima, M. D.; Fang, S. Sound of Carbon Nanotube Assemblies. *J. Appl. Phys.* **2009**, *106*, 124311.
26. Aliev, A. E.; Lima, M. D.; Fang, S.; Baughman, R. H. Underwater Sound Generation Using Carbon Nanotube Projectors. *Nano Lett.* **2010**, *10*, 2374–2380.
27. Xiao, L.; Liu, P.; Liu, L.; Li, Q.; Feng, Z.; Fan, S.; Jiang, K. High Frequency Response of Carbon Nanotube Thin Film Speaker in Gases. *J. Appl. Phys.* **2011**, *110*, 084311.
28. Wei, Y.; Lin, X.; Jiang, K.; Liu, P.; Li, Q.; Fan, S. Thermoacoustic Chips with Carbon Nanotube Thin Yarn Arrays. *Nano Lett.* **2013**, *13*, 4795–4801.
29. Suzuki, K.; Sakakibara, S.; Okada, M.; Neo, Y.; Mimura, H.; Inoue, Y.; Murata, T. Study of Carbon-Nanotube Web Thermoacoustic Loud Speakers. *Jpn. J. Appl. Phys.* **2011**, 50.
30. Aliev, A. E.; Gartstein, Y. N.; Baughman, R. H. Increasing the Efficiency of Thermoacoustic Carbon Nanotube Sound Projectors. *Nanotechnology* **2013**, *24*, 235501.
31. Tian, H.; Shu, Y.; Cui, Y.-L.; Mi, W.-T.; Yang, Y.; Xie, D.; Ren, T.-L. Scalable Fabrication of High-Performance and Flexible Graphene Strain Sensors. *Nanoscale* **2013**, *6*, 699–705.
32. El-Kady, M. F.; Strong, V.; Dubin, S.; Kaner, R. B. Laser Scribing of High-Performance and Flexible Graphene-Based Electrochemical Capacitors. *Science* **2012**, *335*, 1326–1330.
33. Strong, V.; Dubin, S.; El-Kady, M. F.; Lech, A.; Wang, Y.; Weiller, B. H.; Kaner, R. B. Patterning and Electronic Tuning of Laser Scribed Graphene for Flexible All-Carbon Devices. *ACS Nano* **2012**, *6*, 1395–1403.
34. El-Kady, M. F.; Kaner, R. B. Scalable Fabrication of High-Power Graphene Micro-supercapacitors for Flexible and On-Chip Energy Storage. *Nat. Commun.* **2013**, *4*, 1475.